Archived version from NCDOCKS Institutional Repository http://libres.uncg.edu/ir/asu/

Appalachian
STATE UNIVERSITY
BOONE, NORTH CAROLINA

A Mechanistic Treatment Of The Dominant Soil Nitrogen Cycling Processes: Model Development, Testing, And Application

By: Maggi, F., **Chuanhai Gu**, Riley, W.J., G.M. Hornberger, R.T. Venterea, T. Xu, N. Spicher, C. Steefel, N.L. Miller and C.M. Oldenburg

Maggi, F., **Gu, Chuanhai,** Riley, W.J., G.M. Hornberger, R.T. Venterea, T. Xu, N. Spicher, C. Steefel, N.L. Miller and C.M. Oldenburg. **(2008)**. "A Mechanistic Treatment Of The Dominant Soil Nitrogen Cycling Processes: Model Development, Testing, And Application," Journal of Geophysical Research, VOL. 113, G02016. Original version available: [**DOI**:10.1029/2007JG000578],[**ISSN**: 0148-0227]

A mechanistic treatment of the dominant soil nitrogen cycling processes: Model development, testing, and application

1. Introduction

[2] The broad impact of NO and N_2O gas emissions on climate change are widely recognized [e.g., *Mosier*, 1998; *Vitousek et al.*, 1997], as are the effects of NO_3^- water contamination on human health [e.g., *Kapoor and Viraraghavan*, 1997] and eutrophication [e.g., *Cloern*, 2001]. Methods for evaluating the impacts of climate change, and fertilizer and water application techniques on N losses in agriculture are needed for both scientific investigations and management to limit N losses [e.g., *Mosier et al.*, 1996; *Matson et al.*, 1998; *Subbarao et al.*, 2006]. In view of the needs for future increases in crop yield for food, fiber, and biofuel production, understanding the processes that regulate losses of solute and gaseous N species assumes even greater importance.

[3] A recent review by *Heinen* [2006] assesses more than fifty empirical models for denitrification based either on potential denitrification (measured as a soil property or computed from organic C dynamics) or first-order decay process. Among these, two largely accepted coarse-scale models such as CENTURY [*Parton et al.*, 1996] and CASA [*Potter et al.*, 1997] have been used for global-scale assessments of nitrogen balance, suggesting a linear relation between the total amount of applied N fertilizer and N available for leaching, plant uptake, and denitrification [e.g., *Mosier*, 2002; *Broadbent and Carlton*, 1979; *Galloway et al.*, 1995]. The validity of some of the model assumptions as well as some of the field measurements on which they are based (flux chambers) have been questioned [*Grant et al.*, 2006] because N losses after fertilization are essentially pulses, i.e., characterized by a rapid increase of N concentration in the liquid and gaseous phases [e.g., *Hutchinson et al.*, 1997; *Scholes et al.*, 1997; *Venterea and Rolston*, 2000b; *Hosono et al.*, 2006].

[4] Recognition that a set of complex nonlinear biophysical relationships governs the behavior of agroecosystem response to fertilizer and water application indicates that a detailed physical and biological process-based modeling

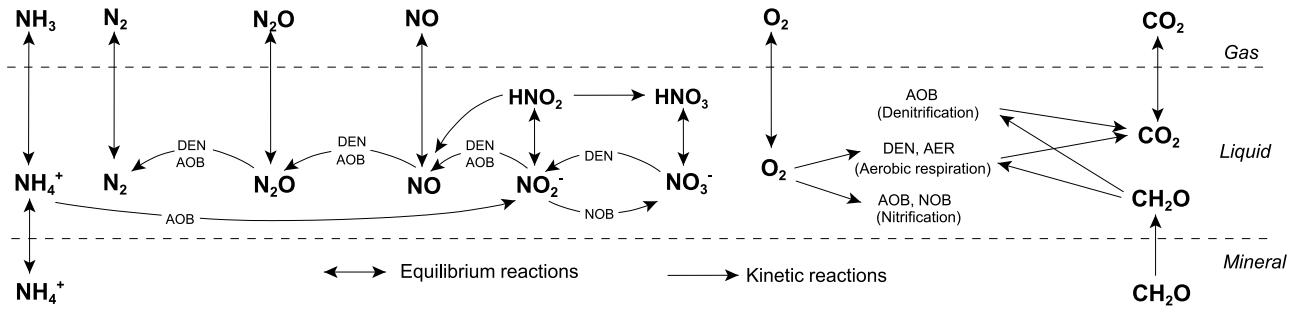

Figure 1. Schematic representation of the chain of biochemical nitrification and denitrification reactions (left side) and microbial respirations (right side). Mineral, liquid, and gaseous domains are separated by dashed lines. AOB, NOB, DEN, and AER stand for ammonia oxidizing bacteria, nitrite oxidizing bacteria, denitrifying bacteria, and aerobic bacteria, respectively.

approach is needed to investigate dynamic system responses. However, a much smaller number of process-based (mechanistic) models have been developed to characterize the soil N cycle. These models are often limited to specific segments of the biogeochemical N cycle, that is, either nitrification or denitrification alone [e.g., *Venterea and Rolston*, 2000a; *Riley and Matson*, 2000; *Hosen et al.*, 2000]. Further, these models typically account for only diffusive transport in the gas or liquid phases [e.g., *Venterea and Rolston*, 2000a; *Garnier et al.*, 2001]. Water dynamics in the vadose zone, including advective transport, is recognized to be important for reactive nutrient transport [e.g., *Simunek and Suarez* 1993], the feedback on soil hydraulic properties and microbial communities [e.g., *Maggi and Porporato*, 2007], and water control on N and C cycles [e.g., *D'Odorico et al.*, 2003]. One of the most complete mechanistic models was presented by *Grant and Pattey* [2003] and used by *Grant et al.* [2006] to investigate questions related to temporal variability in the flux of N gas species at the soil surface in agroecosystems. The Grant and Pattey model does consider all transport contributions in both gas and liquid phases, but neglects important intermediate N compounds such as NO(g) and NO(aq), and HNO_2 and HNO_3, species that precede N_2O formation. HNO_2 and HNO_3 chemical transformations are critical in controlling N cycle transformation rates and outcomes [*Venterea and Rolston*, 2000a], and we explicitly included these transformations in TOUGHREACT-N.

[5] The aim of this work was to adapt the coupled reactive transport model TOUGHREACT [*Xu et al.*, 2005, 2006], which is based on the multiphase and multicomponent model TOUGH2 [*Pruess et al.*, 1999], to investigate the ways in which fine-scale spatial and temporal aspects of the biogeochemical N cycle change with fertilizer application rate, irrigation water volume, and fertilizer application depth. We focus here on capturing the small-scale interplays between physical, biochemical, and hydrological feedbacks controlling competitive interactions among various microbial groups, production rates, partitioning into gaseous and leachate losses, and on the contributions from different pathways to oxidized and reduced N species. The process-based TOUGHREACT-N model includes various nitrification and denitrification pathways, and includes biochemical kinetic reactions and microbial biomass dynamics for various bacterial species, soil moisture dynamics and its effect on microbial processes, advective and diffusive transport, partitioning of N species in the aqueous and gaseous phases, and several equilibrium and kinetic reactions that link the N and C cycles. TOUGHREACT-N, applied here to a one-dimensional soil column, is calibrated with data acquired from a field experiment in Sacramento, California.

[6] Our results indicate that responses are nonlinear both spatially (with the depth) and temporally, calling into question the assumptions of global assessments by empirical models that generally invoke linear relationships [*Heinen*, 2006] between fluxes and both fertilizer and water application.

2. Methods

2.1. Experimental Data

[7] Experimental data were collected from a furrow-irrigated tomato field during July–August 1998 in western Sacramento County, California. Fertilization consisted of an application of anhydrous ammonia, NH_3, injected at 5 cm depth on 1st July, and irrigation occurred on 11th July [*Venterea and Rolston*, 2000b]. Available data consist of water saturation S_θ (volume of water per volume of pores), pH, concentrations of NH_4^+, NO_2^-, and NO_3^- solutes between 0–5 cm and 5–10 cm depth, and NO, N_2O, and CO_2 fluxes measured at various times for 20 days after fertilization (see details in the work by *Venterea and Rolston* [2000a, 2000b] and *Venterea et al.* [2005]).

[8] In the following sections we describe how we have characterized the hydrological, geological, biological, and chemical processes relevant to the agricultural system analyzed here.

2.2. Nitrogen Cycle

[9] The reactions responsible for N transformations are numerous and mainly mediated by a broad gamut of microorganisms that extensively inhabit near-surface soils. These microorganisms can potentially transform N via more than one pathway [e.g., *Wrage et al.*, 2001; *Shrestha et al.*, 2002], and under various conditions of temperature, pH, water content, substrate, and electron acceptor and inhibitor concentrations [e.g., *Knowles*, 1982]. The reaction network used in TOUGHREACT-N is depicted in Figure 1 and described below.

[10] Nitrification of ammonium (NH_4^+ ion) into nitrate (NO_3^- ion) consists of two oxidation reactions mediated

Table 1a. List of Primary Species

Compound	Primary Species
Ion	H^+, HCO_3^-, NH_4^+, NO_2^-, NO_3^-
Molecule	O_2(aq), H_2O, CH_2O, NO(aq), N_2O(aq), N_2(aq)

respectively by ammonia oxidizing autotrophic bacteria (AOB; e.g., *Nitrosomona* and *Nitrosospira*) and by nitrite oxidizing autotrophic bacteria (NOB; e.g., *Nitrobacter* and *Nitrospira*) [e.g., *Salsac et al.*, 1987; *Arp and Stein*, 2003]. AOB and NOB are known to be active in moist soils under oxic conditions, while they become inactive at low soil moisture content and water potential, and under anoxic conditions [e.g., *Rosswall*, 1982; *Rodrigo et al.*, 1997]. In these hostile conditions, nitrification can be performed by heterotrophic nitrifiers (i.e., some fungi and bacteria) [*Prosser*, 1989]. However, their biological functioning is not well understood, and since the soil conditions under investigation are favorable to AOB and NOB, we will neglect heterotrophic nitrification as a first approximation in the current analysis.

[11] Denitrification of NO_3^- ion back to zero-valent dinitrogen N_2 consists of a sequence of redox reactions mainly mediated by heterotrophic denitrifier bacteria (DEN; e.g., *Pseudomonas*, *Thiobacillum*) that consume dissolved organic carbon (DOC) and use NO_3^-, NO_2^-, NO, and N_2O as electron acceptors [e.g., *Payne*, 1973; *Knowles*, 1982; *Rosswall*, 1982]. The metabolism of DEN, with concomitant CO_2 production, is limited by available DOC, and is favored under anoxic conditions while declining under water drought stress. We will assume that some AOB are capable of carrying out part of the denitrification reactions in anoxic conditions by means of the same reactions as DEN [e.g., *Tortoso and Hutchinson*, 1990; *Wrage et al.*, 2001]. Following the experimental and modeling results of *Venterea and Rolston* [2000a], the contribution of chemical decomposition of HNO_2 into HNO_3 and NO was taken into account in TOUGHREACT-N.

[12] In linking the N cycle to part of the C cycle in a simplified manner, we assume that a background organic carbon dissolution sustains a DOC pool as in work by *Li et al.* [1992]. Although DOC is known to comprise a large number of complex and more or less recalcitrant molecules, we consider CH_2O as the available DOC substrate for simplicity [e.g., *Chen and MacQuarrie*, 2004]. In the model, DOC is competitively consumed by AOB and DEN during denitrification, and by other heterotrophic and aerobic microorganisms (AER) during respiration, resulting in CO_2 production.

[13] We do not include dissimilatory nitrate and nitrite reduction into NH_4^+, as this process usually occurs in anaerobic soils [*Knowles*, 1982], which are not prevalent in our study. Oxidation of NO into NO_2^- by heterotrophic and autotrophic bacteria [e.g., *Dunfield and Knowles*, 1997; *Venterea and Rolston*, 2000a, 2000b] is not taken into account explicitly, but lumped in the denitrification rates. Also, we do not include dinitrogen fixation, which mainly occurs by symbiosis between legumes and diazotrophs. Finally, although bioclogging can occur during biomass growth [*Maggi and Porporato*, 2007], we neglect the effect of microbial volume augmentation on soil porosity and its effect on soil-water potential and water flow.

2.3. Chemical and Biological Reactions

[14] To represent the geochemical system in TOUGHREACT-N we select a set of aqueous primary species (Table 1a); these produce secondary species by chemical reactions of aqueous complexation, gas dissolution and exsolution, and solute adsorption and desorption occurring at local equilibrium.

[15] The aqueous concentration C_{wi} of secondary species i determined by aqueous complexation (AC) of primary species of index j at concentration C_{wj} is computed from the mass-action equation

$$\left.\frac{\partial C_{wi}}{\partial t}\right|_{AC} = \frac{1}{\gamma_i^{x_{ji}} K_{ACi}} \prod_j \gamma_j^{x_{ji}} \frac{\partial C_{wj}}{\partial t}, \tag{1}$$

where K_{ACi} is the equilibrium constant (Table 1b and notation list for units), x_{ji} are the stoichiometric coefficients of the reactions in Table 1b, and γ_i and γ_j are the thermodynamic activity coefficients that are solved for during numerical integration of the coupled system.

[16] Gas dissolution and exsolution (GD) rates are calculated by relating the aqueous concentration of a primary or secondary species C_{wi} to its partial pressure, $p_i = C_{gi}RT$, in the gas phase as

$$\left.\frac{\partial C_{wi}}{\partial t}\right|_{GD} = RT \frac{K_{GDi}}{\prod_i \gamma_i^{x_{ji}}} \left.\frac{\partial C_{gi}}{\partial t}\right|_{GD}, \tag{2}$$

where C_{gi} is the gaseous concentration, R and T are the universal gas constant and absolute temperature (here fixed at 293 K), respectively, and K_{GDi} is the equilibrium constant (Table 1b).

Table 1b. Secondary Species Obtained by Equilibrium Kinetic Reactions Described by Equation (1), (2), and (3)[a]

Aqueous Complexation	$\log(K_{AC})$
$OH^- \rightleftarrows H_2O - H^+$	13.99
NH_3(aq) $\rightleftarrows NH_4^+ - H^+$	9.24
$HNO_2 \rightleftarrows H^+ NO_2^-$	−3.22
$HNO_3 \rightleftarrows H^+ NO_3^-$	1.30
$CO_3^{-2} \rightleftarrows HCO_3^- - H^+$	10.32
CO_2(aq) $\rightleftarrows -H_2O + H^+ + HCO_3^-$	−6.34
Gas Dissolution/Exsolution	$\log(K_{GD})$
CO_2(g) $\rightleftarrows -H_2O + H^+ + HCO_3^-$	−7.81
NO(g) $\rightleftarrows$ NO(aq)	−2.76
N_2O(g) $\rightleftarrows$ N_2O(aq)	−1.60
N_2(g) $\rightleftarrows$ N_2(aq)	−3.24
O_2(g) $\rightleftarrows$ O_2(aq)	−2.89
NH_3(g) $\rightleftarrows$ NH_3(aq)	11.04
Solute Adsorption/Desorption	$\log(K_{MA})$
NH_4^+	3

[a]Values of K_{AC}, K_{GD}, and K_{MA} were computed with SUPCRT92 [*Johnson et al.*, 1992] with reference data from *Shock et al.* [1997], as implemented in the EQ3/6 database (Lawrence Livermore National Laboratory, www.llnl.gov).

[17] Adsorption and desorption of solute species to the mineral phase (MA) are computed according to

$$\left.\frac{\partial C_{wi}}{\partial t}\right|_{MA} = \frac{1}{K_{MA} W_M} \frac{\partial W_A}{\partial t}, \tag{3}$$

where K_{MA} is the equilibrium constant (Table 1b), W_A is the weight of sorbate, and W_M is the weight of sorbent [*Langmuir*, 1997]. This equilibrium reaction applies to NH_4^+, which is adsorbed to negatively charged clay particles present in the soil.

[18] All microbially mediated (B) transformations of N species are aqueous reactions. The net variation of concentration of a substrate C_{wi} depends on the rate of production of species i from substrate p by biomass B_p and from consumption of species i during metabolism of biomass B_c, that is

$$\left.\frac{\partial C_{wi}}{\partial t}\right|_{B} = \sum_p \widehat{\mu_{ip}} M_{ip} B_{ip} - \sum_c \widehat{\mu_{ic}} M_{ic} B_{ic}, \tag{4}$$

with $\widehat{\mu_{ip}}$ and $\widehat{\mu_{ic}}$ the maximum specific consumption rates, and M_{ip} and M_{ic} the Michaelis-Menten terms. Regardless of the indices p and c, for a generic substrate i we can write the Michaelis-Menten term as

$$M_i = \frac{C_{wi}}{K_{C_{wi}} + C_{wi}} \frac{e_i}{K_{e_i} + e_i} \frac{K_{I_i}}{K_{I_i} + I_i} f(S_\theta) g(\mathrm{pH}), \tag{5}$$

with e_i and I_i the electron acceptor and inhibitor concentrations, K_{Cwi} and K_{ei} the Michaelis-Menten constants, and K_{Ii} the inhibition constant [*Kindred and Celia*, 1989]. Terms $f(S_\theta)$ and g(pH) are two piecewise linear functions accounting for microbial water and acidity stress. We assume that these functions apply to all microbial populations according to earlier modeling efforts [*Boon and Laundelot*, 1962; *Skopp et al.*, 1990; *Maggi and Porporato*, 2007]

$$f(S_\theta) = \min\{2S_\theta, 1\} \tag{6}$$

$$g(\mathrm{pH}) = \begin{cases} \min\left\{\frac{1}{4}\mathrm{pH} - \frac{3}{4}, -\frac{1}{4}\mathrm{pH} + \frac{11}{4}\right\}, & 3 < \mathrm{pH} < 11; \\ 0, & \text{otherwise.} \end{cases} \tag{7}$$

[19] Equation (4) simplifies for some reactions shown in Figure 1; for instance, for NH_4^+ only the negative term on the right-hand side of equation (4) applies because ammonium is only consumed, while for N_2(aq) only the positive term applies because dinitrogen is only produced.

[20] TOUGHREACT-N models nonbiological N transformations as aqueous reactions. The net variation of concentration C_{wi} depends on the rate of production of species i from species p and from consumption of species i into species c, that is, written using first-order kinetics

$$\left.\frac{\partial C_{wi}}{\partial t}\right|_{NB} = \sum_p \widehat{\eta_{ip}} C_{wp} - \sum_c \widehat{\eta_{ic}} C_{wc}, \tag{8}$$

with $\widehat{\eta_i}$ the maximum specific reaction rate.

2.4. Microbial Biomass Dynamics

[21] The dynamics of each microbial biomass B_i in equation (4) is assumed to satisfy the Monod equation [e.g., *Belser*, 1979]

$$\frac{\partial B_i}{\partial t} = B_i \sum_c \widehat{\mu_{ic}} M_{ic} Y_{ic} - \delta_i B_i, \tag{9}$$

with Y_{ic} the yield coefficients for B_i to grow upon the substrate c, M_{ic} as in equation (5) for each substrate c, and δ_i the biomass death rate. For simplicity, we do not consider here chemotaxis and other concentration-induced mobility mechanisms for the biomass; because of the general nature of TOUGHREACT-N framework, these processes can easily be integrated in future studies.

2.5. Soil Moisture Dynamics

[22] Water flow is modeled in the vertical direction z with the Darcy-Richards equation [*Hillel*, 2004] as implemented in TOUGH2/EOS9 [*Pruess et al.*, 1999]

$$\frac{\partial \theta}{\partial t} = \frac{\partial}{\partial z}\left[K(\theta)\left(\frac{\partial[\psi(\theta)]}{\partial z} + 1\right)\right], \tag{10}$$

where θ is the soils moisture (volume of water per volume of soil), $\psi(\theta)$ and $K(\theta)$ are the water potential and hydraulic conductivity, respectively, computed as functions of the soil type according to *van Genuchten* [1980]. A silt loam is used in TOUGHREACT-N with density of 2600 kg m^{-3}, porosity of 0.6, permeability of $1.82 \cdot 10^{-13}$ m^2, residual water saturation of 0.001, and van Genuchten parameter of 0.62. Different parameters can be used to describe other soils and hydraulic properties.

[23] In the absence of plant root systems in this experiment, we assume that plant-water uptake is negligible within the 20 day timescale examined in this study.

2.6. Chemical Species Transport

[24] Transport of chemical species is modeled by Fickian diffusion in the gas and liquid phases, and advection in the liquid phase. The rate of change of aqueous and gaseous concentrations C_{wi} and C_{gi} for each chemical species i are written as

$$\frac{\partial C_{wi}}{\partial t} = \frac{\partial}{\partial z}\left[D_w \frac{\partial C_{wi}}{\partial z} + v C_{wi}\right] + \sum_k \left.\frac{\partial C_{wi}}{\partial t}\right|_k, \tag{11}$$

$$\frac{\partial C_{gi}}{\partial t} = \frac{\partial}{\partial z}\left[D_g \frac{\partial C_{gi}}{\partial z}\right] + \left.\frac{\partial C_{gi}}{\partial t}\right|_{GD}, \tag{12}$$

where D_{wi} and D_{gi} are the effective diffusion coefficients in the liquid and gaseous phases, respectively. Index $_k$ in equation (11) refers to equations (1), (2), (3), (4), and (8), while subscript *GD* in equation (12) refers to gas dissolution and exsolution. The effective diffusion coefficients D_{wi} and D_{gi} between two adjacent nodes $_1$ and $_2$ are computed for each component $_i$ as [*Pruess et al.*, 1999] (see also http://www-esd.lbl.gov/TOUGH2)

$$D_w = D_w^*\left(2\frac{\phi_1 S_{\theta 1} \cdot \phi_2 S_{\theta 2}}{\phi_1 S_{\theta 1} + \phi_2 S_{\theta 2}}\right)\left(\frac{\tau_{w1} L_1 + \tau_{w2} L_2}{L_1 + L_2}\right), \tag{13}$$

$$D_g = D_g^*\left(2\frac{\phi_1 S_{g1} \cdot \phi_2 S_{g2}}{\phi_1 S_{g1} + \phi_2 S_{g2}}\right)\left(\frac{\tau_{g1} L_1 + \tau_{g2} L_2}{L_1 + L_2}\right), \tag{14}$$

Table 1c. Biological and Nonbiological Reactions of Nitrification and Denitrification[a]

Biological	Mediator	$\widehat{\mu}$*, s^{-1}	$K_C \cdot 10^{-5}$, mol L^{-1}	$K_e \cdot 10^{-5}$, mol L^{-1}	$K_I \cdot 10^{-5}$, mol L^{-1}	$Y \cdot 10^{-5}$ mg mol^{-1}
$NH_4^+ + 3/2\ O_2(aq) \rightarrow NO_2^- + H_2O + 2\ H^+$	AOB	$9.53 \cdot 10^{-6}$(b)	14,8(c)	2.41	0	20
$NO_2^- + 1/2\ O_2(aq) \rightarrow NO_3^-$	NOB	$1.23 \cdot 10^{-5}$(b)	14.8(c)	2.41	0	25
$2NO_3- + CH_2O \rightarrow + 2NO_2^- + CO_2(aq) + H_2O$	DEN	$2.14 \cdot 10^{-5}$(b)	10	11.3(c)	2.52	6.66
$4NO_2^- + CH_2O + 4H^+ \rightarrow 4NO(aq) + CO_2(aq) + 3H_2O$	DEN	$3.19 \cdot 10^{-6}$(b)	10	11.3(c)	2.52	6.66
	AOB	$9.82 \cdot 10^{-7}$(b)	10	11.3(c)	6.15	6.66
$8NO(aq) + 2CH_2O \rightarrow 4N_2O(aq) + 2CO_2(aq) + 2H_2O$	DEN	$8.97 \cdot 10^{-6}$(b)	10	11.3(c)	2.52	6.66
	AOB	$8.87 \cdot 10^{-5}$(b)	10	11.3(c)	6.15	6.66
$4N_2O(aq) + 2CH_2O \rightarrow 4N_2(aq) + 2CO_2(aq) + 2H_2O$	DEN	$1.23 \cdot 10^{-7}$(b)	10	11.3(c)	2.52	6.66
	AOB	$3.38 \cdot 10^{-8}$(b)	10	11.3(c)	6.15	6.66
$CH_2O + O_2(aq) \rightarrow CO_2(aq) + H_2O$	DEN	$2.66 \cdot 10^{-6}$(b)	10	11.3(c)	0	6.66
	AER	$4.49 \cdot 10^{-6}$(b)	10	11.3(c)	0	6.66

Nonbiological	$\widehat{\nu}$ mol L^{-1} s^{-1}
$3NO_2^- + H^+ \rightarrow H_2O + NO_3^- + 2NO(aq)$	$4.08 \cdot 10^{-4}$
% CH_2O production	$9.86 \cdot 10^{-6}$ *
% HCO_3^- production	$3.52 \cdot 10^{-8}$ *

[a]Values of K_C and K_e were adapted from *Riley and Matson* [2000], while values of K_I were adapted from *Kindred and Celia* [1989], values of Y were computed from stoichiometric ratios as in the work by *Xu et al.* [2006]; $\widehat{\eta} = 4.08 \cdot 10^{-4}$ s^{-1} for chemodenitrification was taken from *Venterea and Rolston* [2000a]. Quantities marked with (b) and (c) were used in the sensitivity analysis of section 3.2.

where D_w^* and D_g^* are the diffusion coefficients in the liquid and gas phases, respectively, ϕ is the porosity, S_θ and S_g are the water and gas saturations, respectively, τ_w and τ_g are the tortuosities computed according to *Millington and Quirk* [1961] as $\tau = \phi^{1/3} S^{7/3}$, and L_1 and L_2 are the distances of the two nodes from their interface. While the diffusion coefficient D_w^* is assumed constant for all components ($D_w^* = 6 \cdot 10^{-6}$ $m^2 s^{-1}$), the coefficient D_g^* is assumed to depend on the molecular weight of each component as [*Lasaga*, 1998]

$$D_g^* = \frac{RT}{3\sqrt{2} P N_A d_m^2} \sqrt{8 \frac{RT}{\pi M}}, \tag{15}$$

with $\pi = 3.1415$, $N_A = 6.022 \cdot 10^{23}$ the Avogadro's number, and d_M and M_M the molecular diameter and weight, respectively.

[25] Because we assume that plant roots are absent, we do not model plant uptake of nutrients such as NH_4^+ and NO_3^-. Advective transport in the gas phase is also not considered in this study, but can be taken into account for situations in which temperature and pressure gradients cause significant convective and advective gas flows.

2.7. Initial and Boundary Conditions

[26] The initial soil-water saturation, and primary species and biomass concentrations within the soil column were assigned according to the measured values, or obtained from calibration when unknown (Table 2). Initial concentrations of secondary aqueous and gaseous species were derived from equations (1), (2), and (3).

[27] The bottom boundary condition for soil-water flow was set to keep saturation S_θ = const = 0.5. Evaporation from the soil surface was set equal to 2 mm day^{-1}, while the water-irrigation flux consisted of one event of 10^{-5} L H_2O $m^{-2}s^{-1}$ for one day on day 9 July, followed by a second event of 410^{-5} L H_2O $m^{-2}s^{-1}$ for four days starting on day 10 July.

[28] Partial pressures of the gaseous species at the top of the soil column were kept constant and equal to 0.209 bar for O_2(g), and equal to zero for all other gases. Surface fluxes of NO(g), N_2O(g), N_2(g), CO_2(g), NH_3(g), and O_2(g) were computed from concentration gradients in the form of excess concentrations relative to the atmospheric ones.

3. Results

3.1. Model Calibration

[29] Data from the experiment described in section 2.1 were used to estimate some initial conditions for the primary species (marked with asterisks in Table 2), and some reaction constants and biomass parameters for the biochemical reactions (marked with asterisks in Tables 1c and 1d). Calibration was assisted by PEST software (Parameter ESTimation, from Papadopulos and Associates Inc., www.sspa.com/pest) to minimize the difference between experimental and simulated data of solute concentrations and gas emissions. We refer to the calibration as the reference simulation in the remainder of the paper.

[30] Injection of NH_3 fertilizer in the field experiment corresponded to approximately 12 g NH_3 m^{-2} (120 kg NH_3 ha^{-1}) applied in bands 15 cm width separated by 85 cm, thus corresponding to a concentration of approximately 96 g NH_3 m^{-2} in the top 10 cm of soil column. Fertilization has been conceptualized in TOUGHREACT-N as an initial concentration of 96 g NH_4^+ m^{-2} instead of NH_3, and we have therefore neglected the equilibrium reaction $NH_3 + H^+ \leftrightarrow NH_4^+$. This approach, however, was not supposed to introduce large deviations from real conditions as NH_3 used in the field was injected in the form of solute.

Table 1d. Death Rates for All Microbial Populations[a]

	AOB	NOB	DEN	AER
δ*, s^{-1}	$2.66 \cdot 10^{-6}$	$7.28 \cdot 10^{-7}$	$1.11 \cdot 10^{-6}$	$3.16 \cdot 10^{-7}$

[a]The δ* values were obtained by calibration.

Table 2. Initial Conditions of Water Saturation and Aqueous Concentrations of All Primary Species[a]

	Depth, cm		
	0–5	5–10	10–60
S_θ	0.9	0.95	0.95
pH	5.0	6.0	7.0
O_2(aq), (mol L^{-1}) · 10^{-4}	2.7	2.7	2.7
NH_4^+, (mol L^{-1}) · 10^{-1}	1.2	1.2	0
NO_3^-, (mol L^{-1}) · 10^{-5}	1.0	1.0	1.0
NO_2^-, (mol L^{-1}) · 10^{-5}	1.0	1.0	1.0
NO(aq), mol L^{-1}	0	0	0
N_2O(aq), mol L^{-1}	0	0	0
N_2(aq), mol L^{-1}	0	0	0
HCO_3^-,* (mol L^{-1}) · 10^{-2}	6.2	8.8	0
CH_2O,* (mg L^{-1}) · 10^2	3.0	3.0	3.0
AOB,* mg L^{-1}	25.7	17.1	4.2
NOB,* mg L^{-1}	0.5	0.5	0.5
DEN,* mg L^{-1}	6.0	6.0	7.0
AER,* mg L^{-1}	5.3	1.3	0.3

[a]Values of the species marked with an asterisk were unknown and were selected in the calibration phase.

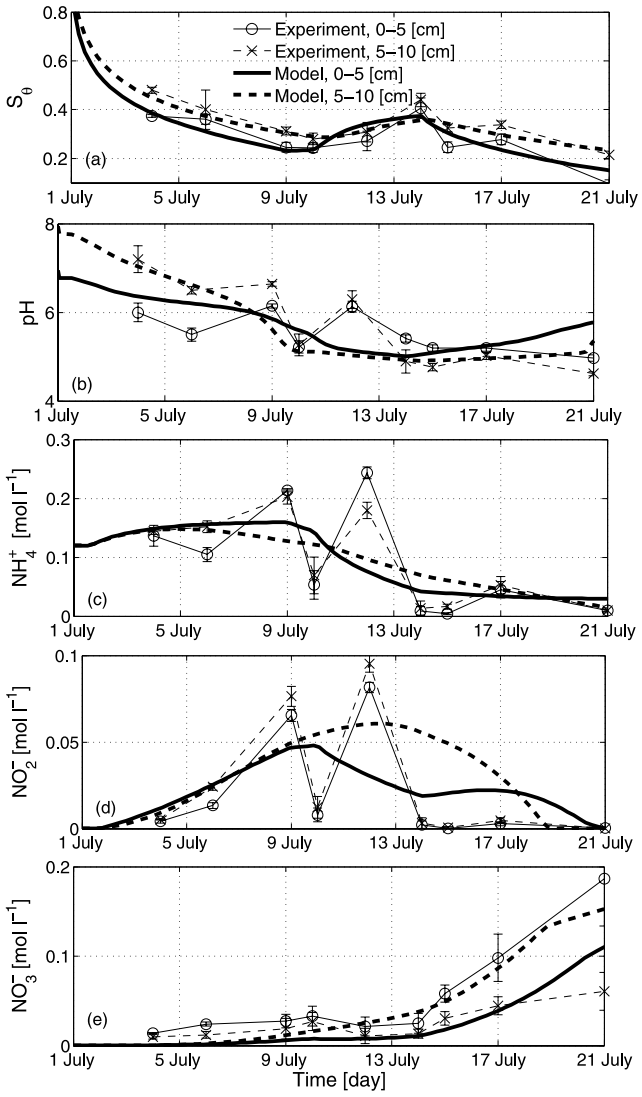

Figure 2. Measured and predicted time evolution of the average soil-water saturation S_θ, pH, NH_4^+, NO_2^-, and NO_3^- solutes at 0–5 cm and 5–10 cm depth.

[31] While noting that S_θ is modeled reasonably well (Figure 2a), all measured solute concentrations in Figures 2b–2e show relatively high fluctuations not predicted by the model. These variations can be partly explained by soil heterogeneity and sampling disturbances. A consistent V-shaped pattern occurred on days 9–12 July in all measurements. No clear explanation has been found for this feature, but it may have been caused by background biogeochemical processes accelerated by irrigation (day 11 July) that have not been monitored in the field experiments, and therefore ignored in our simulation.

[32] A comparison between measured and simulated gas emissions (Figures 3a–3c) shows fluctuations not predicted by TOUGHREACT-N. The overall trend, however, is well modeled, and cumulative fluxes over time of NO(g), N_2O(g), and CO_2(g) match the observations well (Figure 3d).

[33] Over the simulation period, approximately 2.2% of applied fertilizer was lost as NO(g) and 1.3% as N_2O(g). These values agree well with average global estimates from fertilized fields monitored during the growing season [e.g., *Bouwman et al.*, 2002]. Cumulative fluxes of NH_3(g) and N_2(g) gases, and solutes NH_3(aq), NO_2^-, and NO_3^- leaching at 60 cm depth are smaller in terms of mass: approximately 0.2% is lost as NH_3(g), 4.2% as N_2(g), and less than 0.015% as leaching of NH_3(aq), NO_2^-, and NO_3^-.

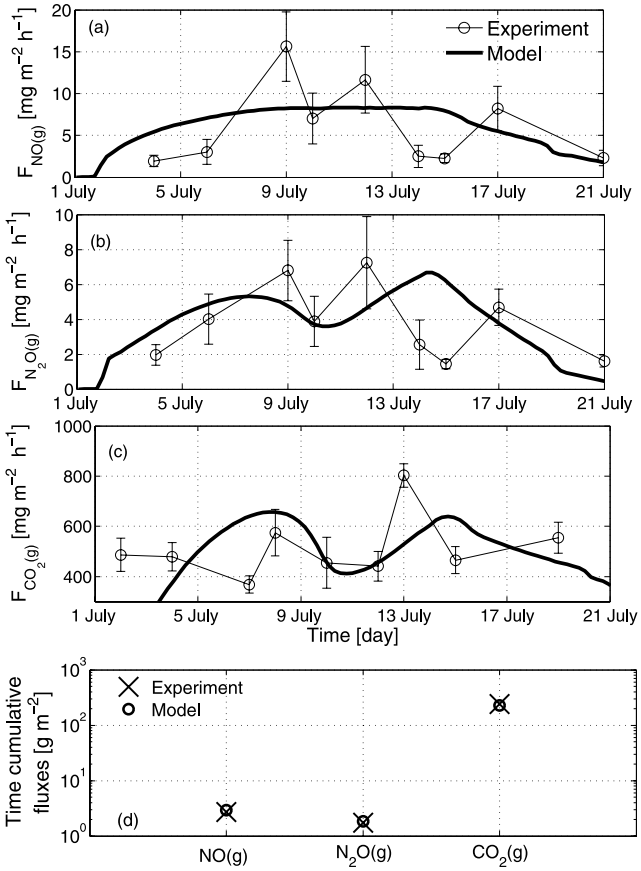

Figure 3. (a–c) Measured and predicted soil gaseous emission of NO(g), N_2O(g), and CO_2(g) over 20 days. (d) Cumulative fluxes over 20-day time of NO(g), N_2O(g), and CO_2(g).

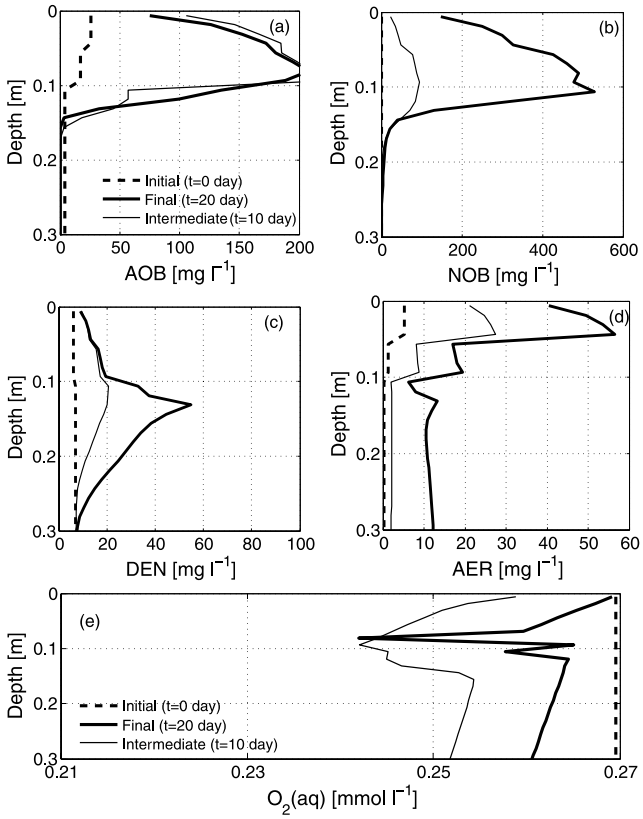

Figure 4. (a–d) Model prediction of the vertical biomass concentrations over time for the four microbial populations used in TOUGHREACT-N. AOB, NOB, DEN, and AER stand for ammonium oxidizing bacteria, nitrite oxidizing bacteria, denitrifying bacteria, and aerobic bacteria, respectively. (e) Model prediction of the vertical profile of O_2(aq) concentration over time.

[34] In addition, we predicted the biomass concentration profiles for the four microbial populations (Figures 4a–4d); although we do not have experimental data with which to compare, stratification of AOB and AER were more dense near the surface, followed by NOB and DEN deeper in the profile which is consistent with earlier works [e.g., *Knowles*, 1982; *Prosser*, 1989]. All four microbial populations reach their peak density within the top 20 cm of soil depth, and their stratification is consistent with the growth-limiting factors of the different populations. In fact, O_2(aq) is rapidly consumed in the top 10 cm of soil by AOB and NOB during nitrification (Figure 4d). Below 10 cm depth, oxygen inhibition (fourth factor in equation (5)) is approximately 0.2 for AOB during nitrifier denitrification, and approximately 0.08 for DEN. High oxygen concentration below 10 cm depth limits DEN growth to a maximum of approximately 50 mg L^{-1} compared with approximately 200 mg L^{-1} and 500 mg L^{-1} of AOB and NOB, respectively.

[35] Experimental observations of fluxes of NH_3(g), N_2(g), NH_3(aq), NO_2^-, and NO_3^-, and biomass distributions were not made. However, we assume these to be relatively correct estimates on the basis of the matching between experimental and modeling data shown (Figures 3 and 2).

3.2. Sensitivity to Rate Constants and Half-Saturation Concentrations

[36] We carried out a sensitivity analysis of the rate constants μ_i and half-saturation concentrations K_C and K_e associated with microbial reactions (see footnote in Table 1c).

[37] First, the μ_i parameters were grouped by microorganismal species (i.e., four groups) and varied by ±5% groupwide, resulting in sixteen simulation experiments. Average, maximum, and minimum time cumulative fluxes of gaseous and leachate N species, computed from the sixteen simulations, were normalized with the corresponding cumulative values from the reference simulation. The same procedure was repeated for parameter variations of ±10%, ±15% and ±20%.

[38] While the average variations did not substantially differ from the reference fluxes, minimum and maximum cumulative fluxes did substantially vary (Figure 5a). The departure was linear with variations up to ±20%; variations of μ_i larger than ±30% caused nonlinear responses for all N species (data not shown). We explain this feature as due to strong feedback processes that both nitrification and denitrification reactions had on oxygen concentration and pH, and, most importantly, on electron acceptor and donor availability. The sensitivity of time-cumulative N_2(g) fluxes were an exception to this behavior, as they appeared nonlinear also for small variations of μ_i. In relative terms, the boundaries represented by the maximum and minimum cumulative fluxes clearly demonstrated that N losses can undergo variations up to ±60% (e.g., N_2O(g), NH_3(g), NH_3(aq)) or higher (e.g., N_2(g)), and that cumulative fluxes of gaseous species were more sensitive than fluxes of aqueous species. The overall response was heterogeneous, with N_2(g) being the most sensitive and CO_2(g) and NH_3(aq) showing the lowest sensitivity to variations in μ_i.

[39] We performed an analogous sensitivity analysis for the half-saturation constant K_{Ci} and K_{ei} (Figure 5b). Here, minimum and maximum cumulative fluxes were generally less sensitive and departed from reference values for a smaller number of N-species compared to variations in μ_i (Figure 5b). In addition, and contrary to Figure 5a, Figure 5b shows that solute NO_2^- and NO_3^- losses were more sensitive to K_{Ci} and K_{ei} than gaseous losses, reaching variations of more than 60%.

3.3. Contributions to N-Gas Emissions by AOB and DEN

[40] While nitrification is performed by AOB only, denitrification is simultaneously performed along two pathways by DEN and AOB. In addition, HNO_2 decomposition (chemodenitrification) contributes to production of NO (Figure 1). To quantify the various contributions to NO(g), N_2O(g), and N_2(g) production and emission, we numerically labeled the NO, N_2O, and N_2 specifically produced by AOB and DEN, and by chemodenitrification.

[41] We found that NO(g) emission was predominantly caused by AOB denitrification (49%) and roughly equally originated by DEN denitrification and HNO_2 decomposition (23% and 28%, respectively). Similarly, we found that N_2O(g) and N_2(g) emissions were largely due to AOB (92% and 85%, respectively) and less a result of DEN activity (8% and 16%, respectively). This result, though appearing counterintuitive at first inspection, can be

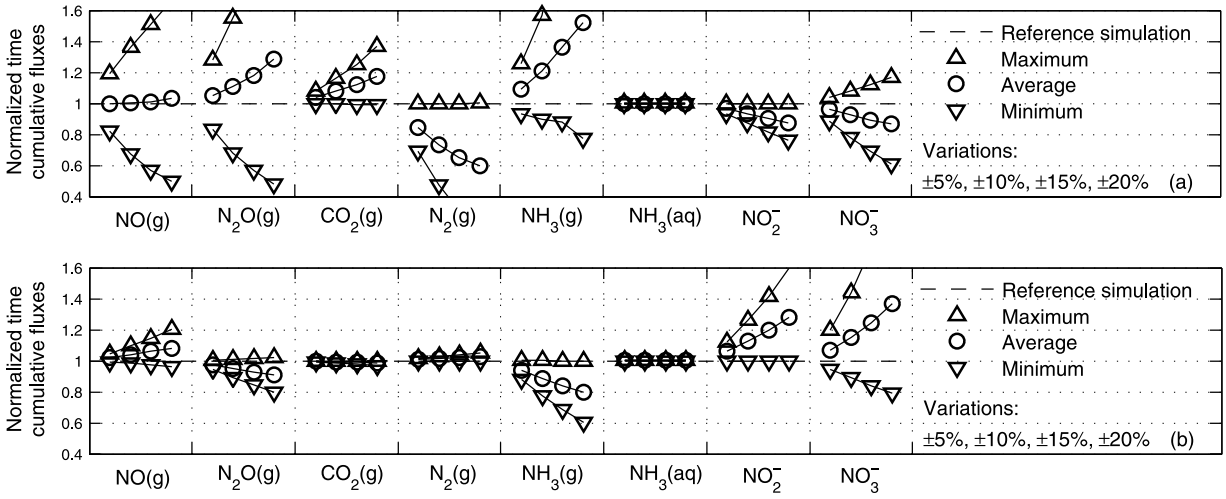

Figure 5. (a) Normalized time cumulative gaseous and leachate losses for various N and C species. Within the bin of each chemical species, four groups of three vertically aligned markers, representing maximum, average, and minimum cumulative fluxes, correspond to the four variations (i.e., ±5%, ±10%, ±15%, and ±20%) in microbial biomass kinetic rate constants μ_i combinatorially applied to each of the four bacterial species represented in Figure 1. (b) Same quantities as in Figure 5a but for variations in half-saturation constants K_{Ci} and K_{ei} marked in Table 1c with the letter b.

explained by an AOB concentration four times higher than that of DEN (Figure 4), a difference due to variations in oxygen content. Oxygen, while acting as a strong inhibitor of DEN denitrification ($K_I/K_I + [O_2(aq)] = 0.08$) and weaker inhibitor of AOB denitrification ($K_I/K_I + [O_2(aq)] = 0.2$), sustains oxidation of NH_4^+ by AOB, thereby favoring AOB growth with respect to DEN, and enabling AOB to denitrify in this oxic condition. The result of this combined metabolic functioning of AOB and DEN, and the effect of oxygen inhibition, explains the high aqueous NO concentration in the top 10 cm of soil, and the stratification of AOB and DEN (Figure 4), the former densely occupying the top 10 cm of the soil column, and the latter occupying the lower 10 cm of soil.

[42] The effect of anoxic microsites, which could favor DEN contribution to N-gas production, is not taken into account explicitly in this model, nor do we have empirical evidence of their presence from the experimental observations. However, a low water saturation ($S_\theta < 0.4$ from day 5 July, Figure 2a) is likely to facilitate oxygen diffusion, and limit the formation of anoxic microsites and denitrifier denitrification [e.g., *Arah and Vinten*, 1995].

3.4. Effect of Fertilizer Application Volume

[43] Cumulative gas and leachate N losses primarily depend on the fertilizer rate and the interaction of various microbial populations. If an increase in fertilizer rate presumably induces an initially higher rate of nitrification and a subsequent higher denitrification rate, nonlinear responses of the biogeochemical functions can result in disproportionate soil N accumulation and loss. To understand how N losses and their partitioning into gas and leachate vary we ran several simulations with varying fertilizer application rates (30–300 kg N ha^{-1}), where 120 kg N ha^{-1} corresponded to the reference application rate. The cumulative gas and leachate fluxes were computed for each fertilizer volume, and normalized with the ones obtained from the reference simulation.

[44] $NH_3(g)$ volatilization increased linearly with fertilizer rate within the range 30–300 kg N ha^{-1} (Figure 6a), while NO(g), $N_2O(g)$, and $N_2(g)$ emissions increased nonlinearly, with $N_2(g)$ showing a hump at about 90 kg N ha^{-1}

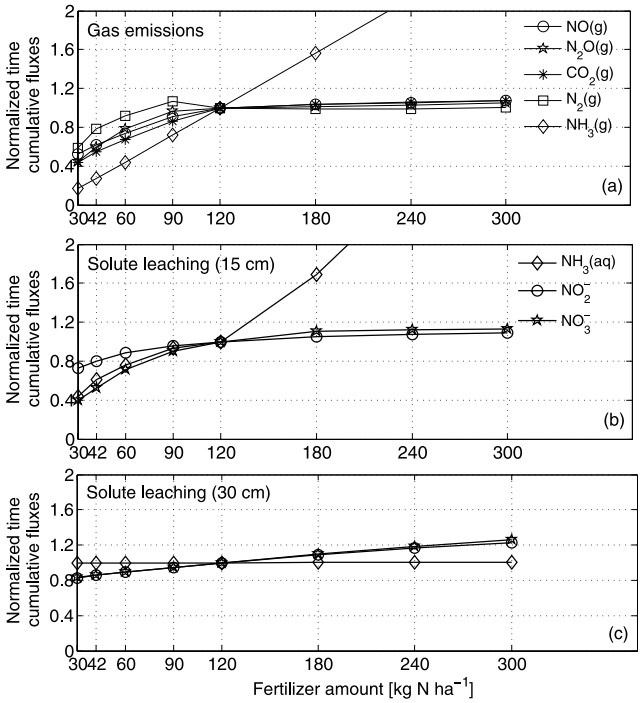

Figure 6. (a) Time cumulative of gaseous fluxes and (b, c) leachate fluxes measured at depths of 15 and 30 cm as functions of fertilizer volume. Fluxes are normalized with the reference ones at fertilizer volume of 120 kg N ha^{-1}.

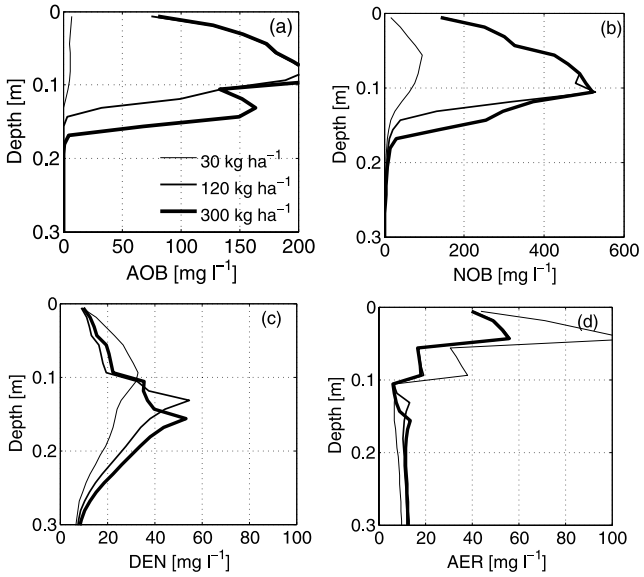

Figure 7. Vertical concentrations of the four microbial populations at day 20 as functions of three fertilizer rates. AOB, NOB, DEN, and AER stand for ammonium oxidizing bacteria, nitrite oxidizing bacteria, denitrifying bacteria, and aerobic bacteria, respectively.

fertilization, and remaining approximately constant for higher fertilizations. Increases of up to three times in NO(g) and N_2O(g) emissions do not compare well with measurements presented by *Harrison et al.* [1995], who reported increases up to approximately four and twenty times, respectively, for fertilizations increasing four times. Among many factors being potential explanations for this difference (i.e., type of soil and microbial composition, cultivation practice, etc.), the fertilizer used by *Harrison et al.* [1995] was ammonium nitrate (NH_4NO_3). This N source, providing substrate for both AOB and DEN simultaneously, may induce faster system response, thereby increasing the cumulative gas emissions over the relatively short timescales of their experiment (e.g., C. Gu et al., Nitrogen losses from different N sources Induced by fertilizer application, submitted to *Journal of Geophysical Research*, 2008).

[45] Cumulative solute leaching increased with fertilizer rate, and decreased with depth owing to the flow rate and timescales (Figures 6b and 6c). At 15 cm depth, NH_3(aq) leaching dominated, increasing nonlinearly with the amount of fertilizer applied between 0 and 10 cm depth. At 60 cm depth, leaching was practically negligible over the short time period simulated (data not shown). In our soil system, and for relatively dry soils and scarce water applications (S_θ is less then 0.4 from day 5 July), N losses occurred almost totally as gas emissions during the 20 day time scale. For simulation periods longer then 20 days, leaching at 60 cm depth increases with irrigation rates (not shown).

[46] Increasing the fertilizer rate from 30 kg N ha^{-1} to the reference value of 120 kg N ha^{-1} strongly impacted the system response, while the relative response for fertilizations between 120 kg N ha^{-1} and 300 kg N ha^{-1} was small (Figure 6). This latter response occurred because nitrification and denitrification rates reached their maxima relative to pH and water saturation controls.

[47] Increased fertilizer application increased the concentrations of AOB and NOB, had little impact on the concentration of DEN, and decreased the concentration of the AER (Figure 7). While faster AOB and NOB growth rates correlated to increases in available substrate, a decrease in AER concentration was due to competition for oxygen, which was more rapidly consumed by AOB during nitrification than by AER during respiration. The location of the peak concentration of each population did not vary substantially within the soil column as a function of fertilizer rate; that is, the profiles shown in Figure 4 were relatively consistent features of this system.

[48] Finally, major N losses occurred as NO(g) and N_2O(g) emissions in the range 0.5–3% and 0.4–2.3% of the applied N, respectively (Table 3a). Losses of all remaining N-species were several orders of magnitude lower than NO(g) and N_2O(g) ($<1.310^{-2}$).

3.5. Effect of Water Irrigation Volume

[49] Irrigation water and soil moisture dynamics are fundamental for the overall microbial activity (equation (5)), and hence for the partitioning between N-solute leaching and N-gas emissions. We simulated water applications ranging from 73 to 588 m^3 ha^{-1} distributed over five days of irrigation, with 146 m^3 ha^{-1} the reference value in the field experiments. All initial conditions were kept identical to the reference simulations.

[50] Cumulative N_2(g) and N_2O(g) emissions increased significantly with irrigation volume, becoming respectively five and three times higher for a water volume four times larger than the reference application (Figure 8a). Emissions of CO_2(g) and NO(g) increased less rapidly, while NH_3(g) volatilization was not affected, as this was instead proportional to the fertilizer rate (Figure 6a) and sensitive to mineral adsorption of NH_4^+.

[51] Predicted time cumulative N-solute fluxes measured at 30 cm depth increased more rapidly than gas emissions (Figure 8b). Leaching of NO_3^- and NO_2^- became respectively more than 100 times the reference values measured in the field, while NH_3(aq) was again not affected. A comparison between Figure 8b and Figure 6c demonstrates how much more important water application is for leaching than

Table 3a. Percent in Mass of Gaseous and Leachate N Losses for Various Fertilizer Applications Under Reference Water Application Computed With Respect to Applied Fertilizer Rate

	kg NH_3^+–N ha^{-1}, g NH_4^+–N m^{-2}							
	30, 24	42, 33	60, 48	90, 72	120, 96	180, 144	240, 191	300, 239
% NO–N	2.83	2.37	1.98	1.64	1.35	0.93	0.71	0.57
% N_2O–N	2.22	2.13	1.96	1.61	1.25	0.85	0.65	0.53

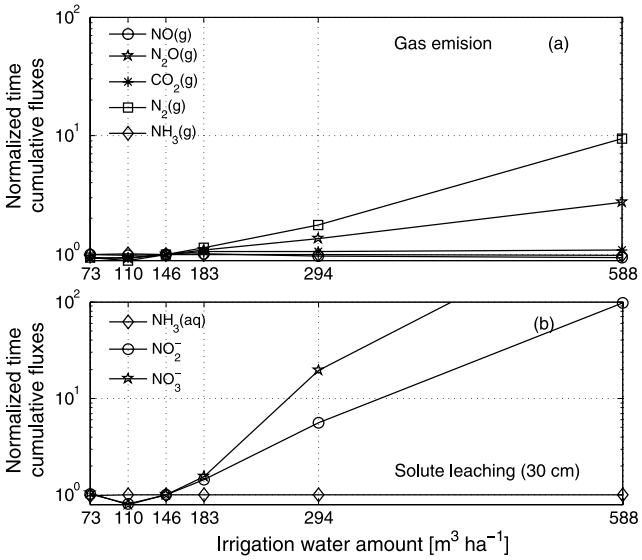

Figure 8. (a) Time cumulative of gaseous fluxes and (b) leachate fluxes as functions of irrigation water volume. All fluxes are normalized with the reference ones at irrigation water volume of 146 m^3 ha^{-1} distributed over 5 days.

fertilizer volume in the first 20 days after fertilization. The response of NO_2^- and NO_3^- leaching at 15 and 60 cm depths followed the same patterns as shown for 30 cm depth (data not shown).

[52] AOB and NOB concentrations increased slightly for water applications in the range 73–146 m^3 ha^{-1} owing to the effect of $f(S_\theta)$ (equation (5)), and decreased for water applications larger than 146 m^3 ha^{-1} (Figure 9). Conversely, DEN and AER concentrations increased monotonically with water volume. The behavior of the DEN is related to a lower oxygen diffusivity through the soil with higher water saturation. The behavior of the AOB and NOB, especially as compared to that of the AER, was due to feedbacks that occur through competition for and limitation by oxygen.

[53] For the full range of water applications considered, the microbial populations are stratified similarly to the ones already found in the calibration, i.e., with AOB, NOB and AER more dense near surface and DEN more dense between 10 and 20 cm depth (Figure 9).

[54] Major N losses occurred as NO(g) and N_2O(g) emissions, which varied with water application volume within the range 1.23–1.33% and 1.23–3.61%, respectively. Other losses were smaller than 0.058% of the reference fertilizer application volume (Table 3b).

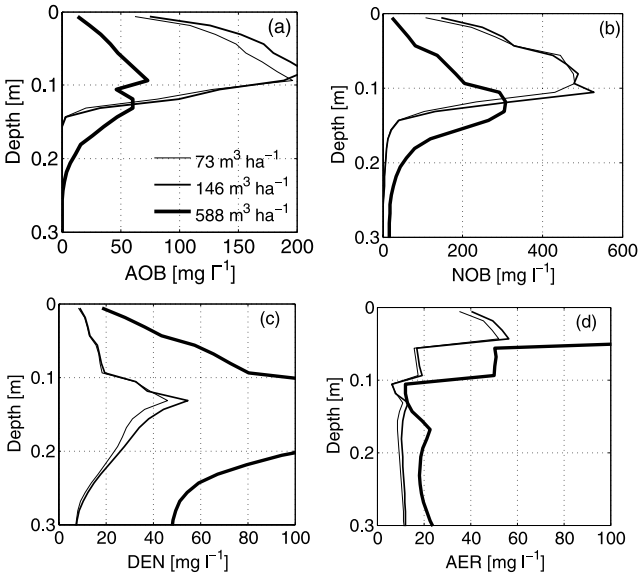

Figure 9. Model prediction of the vertical distributions of the four microbial populations at day 20 as functions of three irrigation water volumes. AOB, NOB, DEN, and AER stand for ammonium oxidizing bacteria, nitrite oxidizing bacteria, denitrifying bacteria, and aerobic bacteria, respectively.

3.6. Effect of Fertilizer Application Depth

[55] Partitioning of N losses into gas emission and solute leaching also depends on the depth of fertilizer application. We ran a series of simulations applying the same volume of fertilizer as in the reference simulation, but at various depths from 0 to 30 cm. Initial and boundary conditions were unchanged.

[56] Emissions of NH_3(g) decreased with fertilizer application depth owing to lower diffusivity throughout the soil (Figure 10a). N_2(g) and N_2O(g) increased by approximately a factor of 2 when fertilizer was applied between 20 and 30 cm depth. This higher rate of N-gas emission is relatively small compared to the increase of N-solute leaching (Figure 10b), with increases of more than 1000 times in NO_3^- and of 200 times in NO_2^- at the 30-cm depth.

[57] The fertilizer application depth had substantial impacts on the structure and stratification of the microbial biomass across the vertical soil profile (Figure 11). AER tended to occupy the top soil depth as in all previous analyses. The spatial distribution of AOB and NOB, which require ammonia (AOB) and nitrite (NOB) for metabolism, correlated to the depth of fertilizer application. For application depths lower than approximately 5–15 cm, denitrifiers tended to stratify and occupy more space above the AOB and NOB. Because the DEN were more dense near the surface for deeper application depths, there was a slight increase in the cumulative emissions of N_2(g) and N_2O(g) for increasing fertilizer application depth (Figure 10a). Though this inversion in microbial spatial distribution persisted over the 20 day timescale, it is expected to revert for longer timescale because of oxygen inhibition on DEN.

[58] Finally, emissions of NO(g) and N_2O(g) increased with fertilizer application depth within the ranges 0.94–1.42% and 1.21–2.92%, respectively (Table 3c). Losses of

Table 3b. Percent in Mass of Gaseous and Leachate N Losses for Various Water Application Volumes Under Reference Fertilization Volume With Respect to Reference Applied Fertilizer Rate

	Water Application Volume, m^3 H_2O ha^{-1}					
	73	110	146	183	294	588
% NO–N	1.31	1.29	1.32	1.33	1.28	1.23
% N_2O–N	1.23	1.21	1.32	1.43	1.77	3.61

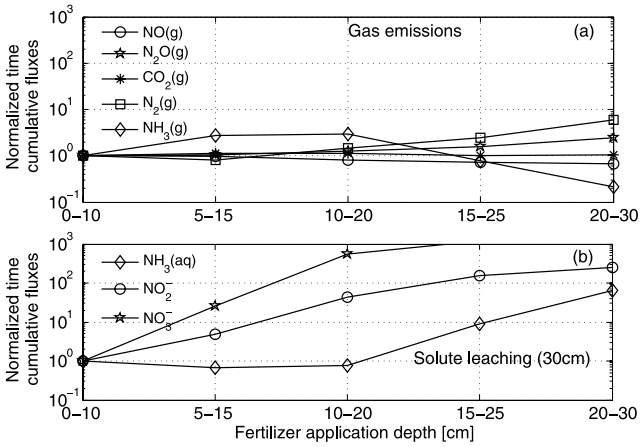

Figure 10. (a) Time cumulative gaseous and (b) leachate fluxes as functions of fertilizer application depth. All fluxes are normalized with the reference ones.

all other N species represented less then 0.04% of the total nitrogen mass of the reference application.

4. Conclusions

[59] After application of mineral N-based fertilizers, relatively rapid reactions mediated by soil microbial consortia produce NO_2^-, NO_3^-, NO, N_2O, and N_2 along various pathways. Initially these species accumulate in the vadose zone near the point of fertilizer application. Fluxes of soil moisture cause excess NO_2^- and NO_3^- to percolate to groundwater, while NH_3, NO, N_2O, and N_2 are released to the atmosphere. While there are other N cycle processes believed to be important under certain conditions (e.g., dissimilatory nitrate reduction), we believe we have characterized the currently understood important hydrological, geological, biological, and chemical processes relevant to the agricultural system analyzed here. We have encompassed these processes in a mechanistic, process-based model complementary to many coarse-scale models for nitrification and denitrification, and have analyzed the small time and space system response to fertilizer and water application.

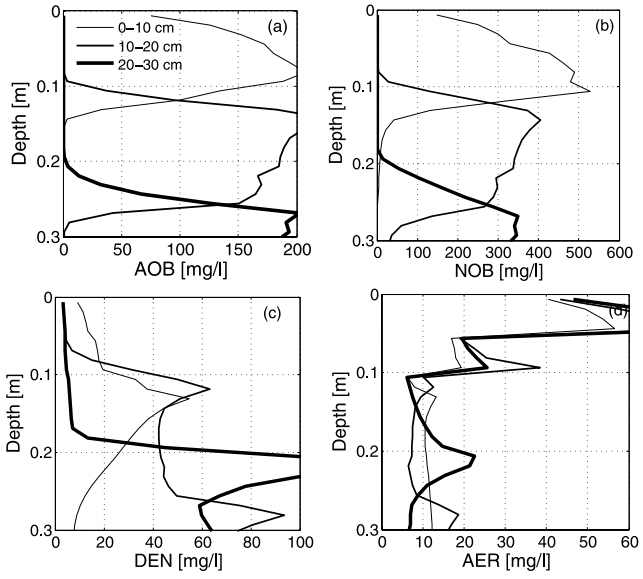

Figure 11. Model prediction of the vertical distributions of the four microbial populations at day 20 as functions of three fertilizer application depths. AOB, NOB, DEN, and AER stand for ammonium oxidizing bacteria, nitrite oxidizing bacteria, denitrifying bacteria, and aerobic bacteria, respectively.

Table 3c. Percent in Mass of Gaseous and Leachate N Losses for Various Fertilizer Application Depths Under Reference Fertilizer and Water Application Volumes With Respect to Applied Fertilizer Rate

	Fertilizer Application Depth, cm				
	0–10	5–15	10–20	15–25	20–30
% NO–N	1.42	1.36	1.15	1.02	0.94
% N_2O–N	1.21	1.27	1.52	1.88	2.92

[60] In all cases investigated here, gaseous N losses were the major pathways for N release to the wider environment, while leaching remained small. However, if water applications were increased then leaching of nitrite and nitrate increased by more than an order of magnitude, while gaseous losses increased by a factor of four. Increasing the fertilizer application depth caused a decrease in gaseous emissions, but leaching increased by approximately two orders of magnitude. The microbial response varied substantially under the same practices, showing variations of up to a factor of five in concentration as a function of fertilizer rate, a factor of four as a function of water volume, and substantial variations in spatial distribution with increased fertilizer application depth.

[61] TOUGHREACT-N has given promising evidence that mechanistic models can provide important tools for assessing the effects of agricultural practices on nitrogen balance and losses, and we foresee further applications of TOUGHREACT-N to investigate the effects of various N sources on N balance and cycling, expanding its functionalities over larger time and length scales.

Notation

C_w aqueous concentration, mol L^{-3}.
C_g gaseous concentration, mol L^{-3}.
d_M molecular diameter, m.
D_w effective diffusion coefficient in the liquid phase, $m^2\ s^{-1}$.
D_g effective diffusion coefficient in the gas phase, $m^2\ s^{-1}$.
e electron donor concentration, mol L^{-3}.
F_x flux of component x, mg $m^{-2}\ s^{-1}$.
K hydraulic conductivity, m s^{-1}.
K_C substrate half-saturation concentration, mol L^{-3}.
K_e electron donor half-saturation, mol L^{-3}.
K_{AC} aqueous complexation constant.
K_{CG} gas dissolution/exsolution constant, mol J^{-1}.
K_{MA} mineral adsorption/desorption constant.
K_I inhibitor half-saturation concentration, mol L^{-3}.
M_M molecular weight, kg mol^{-1}.

N_A Avogadro's number (= 6.022 10^{23}).
p partial pressure, bar.
pH water acidity.
R universal gas constant (= 8.314), $JK^{-1}mol^{-1}$.
S_θ water saturation.
t time [s].
Y biomass yield coefficient, mg mol^{-1}.
W_A weight of sorbate, kg.
W_M weight of sorbent, kg.
δ biomass death rate, s^{-1}.
ψ water potential, m H_2O.
$\widehat{\mu}$ specific consumption rate (biological), mol mg^{-1} s^{-1}.
$\widehat{\eta}$ specific consumption rate (chemical), s^{-1}.
θ soil moisture.
AOB ammonium oxidizer bacteria.
NOB nitrite oxidizer bacteria.
DEN denitrifier bacteria.
AER (other) aerobic bacteria.
$_{AC}$ subscript for aqueous complexation.
$_{GD}$ subscript for gas dissolution and exsolution.
$_{MA}$ subscript for mineral adsorption and desorption.

[62] **Acknowledgments.** This work was supported by Laboratory Directed Research and Development (LDRD) funding from Berkeley Lab, provided by the Director, Office of Science, of the U.S. Department of Energy under contract DE-AC02-05CH11231. The authors also acknowledge the Berkeley Water Center, Yoram Rubin (University of California, Berkeley), and the late Bo Bodvarsson (Lawrence Berkeley National Laboratory) for making this project possible.

References

Arah, J. R. M., and A. J. A. Vinten (1995), Simplified models of anoxia and denitrification in aggregated and simple structured soils, *Eur. J. Soil Sci.*, *46*, 507–517.

Arp, D. J., and L. Y. Stein (2003), Metabolism of inorganic N compounds by ammonia-oxidizing bacteria, *Crit. Rev. Biochem. Mol. Biol.*, *38*, 471–494.

Belser, L. W. (1979), Population ecology of nitrifying bacteria, *Ann. Rev. Microbiol.*, *33*, 309–333.

Boon, B., and H. Laundelot (1962), Kinetics of nitrite oxidation by *Nitrobacter winogradskyi*, *Biochem. J.*, *85*, 440–447.

Bouwman, A. F., L. J. M. Boumans, and N. H. Batjes (2002), Modeling global annual N_2O and NO emissions from fertilized fields, *Global Biogeochem. Cycles*, *16*(4), 1080, doi:10.1029/2001GB001812.

Broadbent, F. E., and A. B. Carlton (1979), Field trials with isotopically labeled nitrogen fertilizer, in *Nitrogen in the Environment*, edited by D. R. Nielsen and J. G. MacDonald, pp. 1–43, Academic Press, San Diego, Calif.

Chen, D. J. Z., and K. T. B. MacQuarrie (2004), Numerical simulation of organic carbon, nitrate, and nitrogen isotope behavior during denitrification in a riparian zone, *J. Hydrol.*, *293*, 235–254.

Cloern, J. E. (2001), Our evolving conceptual model of the coastal eutrophication problem, *Mar. Ecol. Prog. Ser.*, *210*, 223–253.

D'Odorico, P., A. Porporato, F. Laio, and I. Rodriguez-Iturbe (2003), Hydrologic controls on soil carbon and nitrogen cycles II. A case study, *Adv. Water Resour.*, *26*(1), 59–70.

Dunfield, P. F., and R. Knowles (1997), Biological oxidation of nitric oxide in a humisol, *Biol. Fertil. Soils*, *24*, 294–300.

Galloway, J. N., W. H. Schlesinger, H. Levy II, A. Michaelis, and J. L. Schnoor (1995), Nitrogen fixation: Anthropogenic enhancement-environmental response, *Global Biogeochem. Cycles*, *9*(2), 235–252.

Garnier, P., C. Neel, B. Mary, and F. Lafolie (2001), Evaluation of nitrogen transport and transformation model in a bare soil, *Eur. J. Soil Sci.*, *52*, 253–268.

Grant, R. F., and E. Pattey (2003), Modelling variability in N2O emissions from fertilized agricultural fields, *Soil Biol. Biochem.*, *35*, 225–243.

Grant, R. F., E. Pattey, T. W. Goddard, L. M. Kryzanowsky, and H. Puurveen (2006), Modeling the effect of fertilizer application rate on nitrous oxide emissions, *Soil Sci. Soc. Am. J.*, *70*, 235–248.

Harrison, R. M., S. Yamulki, K. W. T. Goulding, and C. P. Webster (1995), Effect of fertilizer application on NO and N_2O fluxes from agricultural fields, *J. Geophys. Res.*, *100*(D12), 25,923–25,931.

Heinen, M. (2006), Simplified denitrification models: Overview and properties, *Geoderma*, *133*, 444–463.

Hillel, D. (2004), *Introduction to Environmental Soil Physics*, Elsevier, Amsterdam.

Hosen, Y., H. Tsuruta, and K. Minami (2000), Effect of depth of NO and N_2O productions in soil and their emission rates to the atmosphere: Analysis by simulation model, *Nutr. Cycl. Agroecosyst.*, *57*, 83–98.

Hosono, T., N. Hosoi, H. Akiyama, and H. Tsuruta (2006), Measurements of N_2O and NO emissions during tomato cultivation using a flow-through chamber system in a glasshouse, *Nutr. Cycl. Agroecosyst.*, *75*, 115–134.

Hutchinson, G. L., M. F. Vigil, J. W. Doran, and A. Kessavalou (1997), Coarse-scale soil-atmosphere NOx exchange modeling: Status and limitations, *Nutr. Cycl. Agroecosyst.*, *48*, 25–35.

Johnson, J. W., E. H. Oelkers, and H. C. Helgeson (1992), SUPCRT92—A software package for calculating the standard molal thermodynamic properties of minerals, gases, aqueous species, and reactions from 1-bar to 5000-bar and 0-degrees-C to 1000-degrees-C, *Comput. Geosci.*, *18*(7), 899–947.

Kapoor, A., and T. Viraraghavan (1997), Nitrate removal from drinking water: Review, *J. Environ. Eng.*, *123*(4), 371–380.

Kindred, J. S., and M. A. Celia (1989), Contaminant transport and biodegradation: 2. Conceptual model and test simulations, *Water Resour. Res.*, *25*(6), 1149–1159.

Knowles, R. (1982), Denitrification, *Microbiol. Rev., Mar*, *46*, 43–70.

Langmuir, D. (1997), *Aqueous Environmental Geochemistry*, Prentice-Hall, Upper Saddle River, N. J.

Lasaga, A. C. (1998), *Kinetic Theory in the Earth Sciences*, Princeton Univ. Press, Princeton, N. J.

Li, C., S. Frolking, and T. A. Frolking (1992), A model of nitrous oxide evolution from soil driven by rainfall events. 1. Model structure and sensitivity, *J. Geophys. Res.*, *97*(D9), 9759–9776.

Maggi, F., and A. Porporato (2007), Coupled moisture and microbial dynamics in unsaturated soils, *Water Resour. Res.*, *43*, W07444, doi:10.1029/2006WR005367.

Matson, P. A., R. Naylor, and I. Ortiz-Monasterio (1998), Integration of environmental, agronomic, and economic aspects of fertilizer management, *Science*, *280*(5360), 112–115.

Millington, R. J., and J. P. Quirk (1961), Permeability of porous solids, *Trans. Faraday Soc.*, *57*, 1200–1207.

Mosier, A. G. (1998), Soil processes and global change, *Biol. Fertil. Soils*, *27*, 221–229.

Mosier, A. G. (2002), Environmental challenges associated with needed increases in global nitrogen fixation, *Nutr. Cycling Agroecosyst.*, *63*, 101–116.

Mosier, A. G., J. M. Duxbury, J. R. Freney, O. Heinemeyer, and K. Minami (1996), Nitrous oxide emission from agricultural fields: Assessment, measurement and mitigation, *Plant Soil*, *181*, 95–108.

Parton, W. J., A. R. Mosier, D. S. Ojima, D. W. Valentine, D. S. Schimel, K. Weier, and A. E. Kulmala (1996), Generalized model for N_2 and N_2O production from nitrification and denitrification, *Global Biogeochem. Cycles*, *10*(3), 401–412.

Payne, W. J. (1973), Reduction of nitrogenous oxides by microorganisms, *Bacteriol. Rev.*, *37*, 409–452.

Potter, C. S., R. H. Riley, and S. A. Klooster (1997), Simulation modeling of nitrogen traces gas emission along an age gradient of tropical forest soils, *Ecol. Modell.*, *97*, 179–196.

Prosser, J. I. (1989), Autotrophic nitrification in bacteria, in *Advances in Microbial Physiology*, vol. 30, edited by A. H. Rose and D. W. Tempest, pp. 125–181, Academic, San Diego, Calif.

Pruess, K., C. Oldenburg, and G. Moridis (1999), TOUGH2 user's guide, version 2.0., *Rep. LBL-43134*, 192 pp., Lawrence Berkeley Natl. Lab., Berkeley, Calif.

Riley, W. J., and P. A. Matson (2000), NLOSS: A mechanistic model of denitrified N_2O and N_2 evolution from soil, *Soil Sci.*, *165*, 237–249.

Rodrigo, A., S. Recous, C. Neel, and B. Mary (1997), Modelling temperature and moisture effects on C-N transformations in soils: Comparison of nine models, *Ecol. Modell.*, *102*, 325–339.

Rosswall, T. (1982), Microbiological regulation of the biogeochemical nitrogen cycle, *Plant Soil*, *67*, 15–34.

Salsac, L., S. Chaillou, J.-F. Morot-Gaudry, C. Lesaint, and E. Jolivet (1987), Nitrate and ammonium nutrition in plants, *Plant Physiol. Biochem.*, *25*(6), 805–812.

Scholes, M. C., R. Martin, R. J. Scholes, D. Parsons, and E. Winstead (1997), NO and N_2O emissions from savanna soils following the first simulated rains of the season, *Nutr. Cycling Agroecosyst.*, *48*, 115–122.

Shock, E. L., D. C. Sassani, M. Willis, and D. A. Sverjensky (1997), Inorganic species in geologic fluids: Correlations among standard molal thermodynamic properties of aqueous ions and hydroxide complexes, *Geochim. Cosmochim. Acta*, *61*, 907–950.

Shrestha, N. K., S. Hadano, T. Kamachi, and I. Okura (2002), Dinitrogen production from ammonia by *Nitrosomonas europea*, *Appl. Catal.*, *237*, 33–39.

Simunek, J., and D. L. Suarez (1993), Modeling of carbon dioxide transport and production in soil 1. Model development, *Water Resour. Res.*, *29*(2), 487–497.

Skopp, J., M. D. Jawson, and J. W. Doran (1990), Steady-state aerobic microbial activity as a fiunction of soil-water content, *Soil Sci. Soc. Am. J.*, *54*(6), 1619–1625.

Subbarao, G. V., K. L. Sahrawat, W. L. Berry, K. Nakahara, T. Ishikawa, T. Watanabe, K. Suenaga, M. Rondon, and I. M. Rao (2006), Scope and strategies for regulation of nitrification in agricultural systems—Challenges and opportunities, *Crit. Rev. Plant Sci.*, *25*, 303–335.

Tortoso, A. C., and L. Hutchinson (1990), Contributions of autotrophic and heterotrophic nitrifiers to soil NO and N_2O emissions, *Appl. Environ. Microbiol.*, *56*, 1799–1805.

van Genuchten, M. T. (1980), A closed-form equation for predicting the hydraulic conductivity of unsaturated soils, *Soil Sci. Soc. Am. J.*, *44*, 892–897.

Venterea, R. T., and D. E. Rolston (2000a), Mechanistic modeling of nitrite accumulation and nitrogen oxide emission during nitrification, *J. Environ. Qual.*, *29*(6), 1741–1751.

Venterea, R. T., and D. E. Rolston (2000b), Nitric and nitrous oxide emissions following fertilizer application to agricultural soil: Biotic and abiotic mechanisms and kinetics, *J. Geophys. Res.*, *105*(D12), 15,117–15,129.

Venterea, R. T., M. Burger, and K. A. Spokas (2005), Nitrogen oxide and methane emissions under varying tillage and fertilizer management, *J. Environ. Qual.*, *34*, 1467–1477.

Vitousek, P. M., J. D. Aber, R. W. Howarth, G. E. Linkens, P. A. Matson, D. W. Schindler, W. H. Schlesinger, and D. G. Tilman (1997), Human alteration of the global nitrogen cycle: Sources and consequences, *Ecol. Appl.*, *7*(3), 737–750.

Wrage, N., G. L. Velthof, M. L. van Beusichem, and O. Oenema (2001), Role of nitrifier denitrification in the production of nitrous oxide, *Soil Biol. Biochem.*, *33*, 1723–1732.

Xu, T., E. Sonnenthal, N. Spycher, and K. Pruess (2005), TOUGHREACT user's guide: A simulation program for non-isothermal multiphase reactive geochemical transport in variable saturated geologic media, *Rep. LBNL-55460*, 192 pp., Lawrence Berkeley Natl. Lab., Berkeley, Calif.

Xu, T., E. L. Sonnenthal, N. Spycher, and K. Pruess (2006), TOUGHREACT—A simulation program for non-isothermal multiphase reactive geochemical transport in variably saturated geologic media: Applications to geothermal injectivity and CO_2 geological sequestration, *Comput. Geosci.*, *32*(2), 145–165.

C. Gu and F. Maggi, Berkeley Water Center, Civil and Environmental Engineering, University of California, Berkeley, 413 O'Brien Hall, Berkeley, CA 94720-1710, USA. (fmaggi@berkeley.edu)

G. M. Hornberger, Department of Environmental Sciences, University of Virginia, PO Box 400123, Charlottesville, VA 22904-4123, USA.

N. L. Miller, C. M. Oldenburg, W. J. Riley, N. Spycher, C. Steefel, and T. Xu, Earth Sciences Division, Lawrence Berkeley National Laboratory, Berkeley, CA 94720, USA.

R. T. Venterea, Soil and Water Management Research Unit, USDA-Agricultural Research Service, 439 Borlaug Hall, 1991 Upper Buford Circle, St. Paul, MN 55108, USA.